Title

Effects of ICG concentration on the optical properties of erythrocyte-derived nano-vectors

ISBN

9781628414318

Authors

Tang, Jack
Bahmani, Baharak
Burns, Joshua
et al.

Publication Date

2015-03-11

DOI

10.1117/12.2079796

Effects of ICG concentration on the optical properties of erythrocyte-derived nano-vectors

Jack Tang[1], Baharak Bahmani[1], Joshua Burns[1], Vicente Nuñez[1], Jenny Mac[2], Danielle Bacon[1], Valentine Vullev[1], Victor Sun[3], Wangcun Jia[3], J. S. Nelson[3], Bahman Anvari[1,3]
[1]Department of Bioengineering, University of California, Riverside, Riverside, CA 92521 U.S.A.
[2]Department of Biochemistry, University of California, Riverside, Riverside, CA 92521 U.S.A.
[3]Beckman Laser Institute & Medical Clinic, University of California, Irvine, Irvine, CA 92617 U.S.A.

ABSTRACT

Erythrocyte-based nanoparticle platforms can offer long circulation times not offered by traditional drug delivery methods. We have developed a novel erythrocyte-based nanoparticle doped with indocyanine green (ICG), the only FDA-approved near-infrared chromophore. Here, we report on the absorption and fluorescence emission characteristics of these nanoparticles fabricated using ICG concentrations in the range of 161-323 μM. These nanoparticles may serve as biocompatible optical materials for various clinical imaging and phototherapeutic applications.

KEYWORD LIST: Cancer, dynamic light scattering, fluorescence, indocyanine green, nanoparticle, phototherapy, spectroscopy, theranostic

INTRODUCTION

Conversion of light into other forms of energy has formed the basis for many biomedical applications such as imaging, photothermal therapy, and photodynamic therapy (PDT). The near-infrared (NIR) wavelengths are well-suited for such applications because biological materials absorb minimally, and there is reduced scattering in this spectral region (650-1450 nm)[1]. Thus, deep tissue penetration can be achieved using these wavelengths (λ).

Indocyanine green (ICG), an FDA-approved NIR chromophore has had a long history of usage in clinical applications. It has been used since the 1950s for characterizing valvular and septal defects[2], measuring cardiac output[3], assessing liver function[4], and ophthalmic angiography[5-7]. ICG has also been approved for measurement of cerebral blood flow in the European Union.[8] Other applications of ICG under investigation include sentinel lymph node mapping of breast[9], cervical[10, 11], prostate[12], and skin[13, 14] cancers. It is also reported for investigational studies in PDT of choroidal disease[15], and colon cancers[16].

Despite the widespread utility of ICG in clinical medicine, its drawbacks are its short half-life in the vasculature (≈2-4 minutes), and exclusive uptake by the liver prior to excretion in the bile[17]. Due to its amphipathic nature, ICG can non-specifically bind to various biomolecules in the vasculature, such as albumin, and high- and low-density lipoproteins. Thus, the potential of free-ICG as a theranostic agent remains limited for medical procedures that require extended vascular circulation time. Encapsulation of ICG within polymer hydrogels[18], viral capsids[19], and erythrocytes[17, 20], have been investigated in order to extend the vascular circulation time of ICG. Our group has reported a polymer-based nanoparticle that enhanced the fluorescence image contrast of circulation for up to 90 minutes in mice[18].

In this study, we investigate the effect of ICG concentration, in the range of 161-323 μM, on the absorption and fluorescence characteristics of erythrocyte-derived ICG carriers. We refer to these nanoparticles as near-infrared erythrocyte-mimicking transducers (NETs). Currently, there are no FDA-approved nanocarriers for use in biomedical applications[17]. The approved status of free-ICG for imaging applications, and previous clinical studies using erythrocyte-based drug-delivery, can potentially make NETs a promising technology for clinical translation.

MATERIALS AND METHODS

Fabrication of NETs

Whole CD-1 mouse blood was drawn by cardiac puncture and chilled to 4°C. Cold whole blood was centrifuged at 800 relative centrifugal force (rcf) for five minutes at 4°C to separate the plasma from the packed RBCs (the packed RBCs

Bioinspired, Biointegrated, Bioengineered Photonic Devices III, edited by Luke P. Lee, John A. Rogers, Seok Hyun Andy Yun, Proc. of SPIE Vol. 9341, 93410H · © 2015 SPIE · CCC code: 1605-7422/15/$18 · doi: 10.1117/12.2079796

occupied approximately half of the total whole blood volume). Then, the plasma was decanted and the packed RBCs were mixed and separated into 250 µL aliquots. We added 1 mL of cold (4°C) 1X PBS to resuspend the RBCs. The RBCs were then washed by centrifugation at 800 rcf for five minutes at 4°C in cold 1X PBS.

Next, we added 1 mL of 0.25X PBS to the washed RBCs to induce hypotonic swelling. This procedure allowed for depletion of hemoglobin from the RBCs. We then separated the hemoglobin from the suspension of erythrocyte ghosts (EGs) by centrifugation at 3000 rcf for five minutes and immediately suspended the EGs in 1 mL of 1X PBS. The volume of EGs was noticeably larger when suspended in 0.25X PBS compared to the volume of EGs suspended in 1X PBS, indicating that swelling did take place.

The EGs were alternatingly incubated in 0.25X PBS and 1X PBS for five minutes in each tonicity. We repeated this three times to remove most of the hemoglobin from the RBCs. This yielded a pink pellet of EGs. The EGs were then serially extruded through track-etched polycarbonate membranes with 0.4 µm pore size using an Avanti Mini-Extruder. Each sample was passed 20 times through the membrane.

ICG was loaded into the nano-sized EGs by incubating them in Sørenson's phosphate buffer (~300 mOsm) with various concentrations of ICG (161-323 µM) for five minutes. The nano-sized NETs were then separated from any remaining free-ICG by centrifugation for fifteen minutes at 10000 rcf. The resulting NETs were then washed at 10000 rcf for 15 minutes at 4°C in 1 mL of 1× PBS.

Characterization of NETs.

The hydrodynamic diameter of NETs was determined by dynamic light scattering (DLS) in polystyrene cuvettes with path length of 1 cm using a Zetasizer NanoZS90 (Malvern Instruments Ltd.). Prior to extrusion, the EGs were measured to be on the order of one micron in diameter. After 20 passes through a porous polycarbonate membrane with 400 nm pore diameter, the extruded EGs had a peak diameter of ~230 nm (Figure 1).

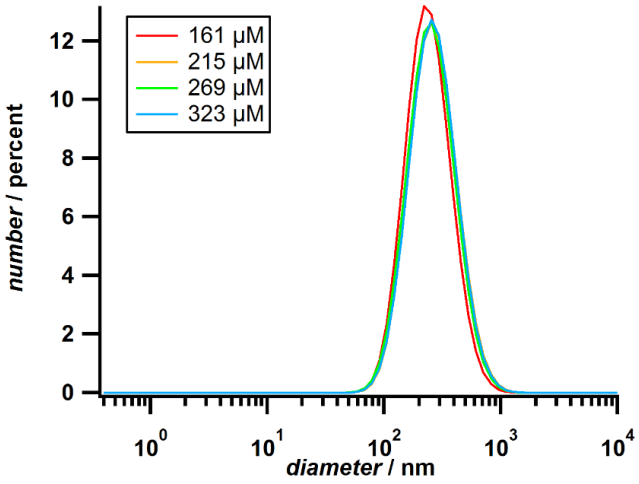

Figure 1: Hydrodynamic diameter distribution of NETs suspended in 1X PBS determined by dynamic light scattering. The peak diameter of NETs is ~230 nm. Datasets were smoothed using 30 passes of a binomial smoothing algorithm in Igor Pro.

Absorbance spectra of NETs (Figure 2) were obtained using a Jasco-V670 UV-Vis spectrophotometer in the range of 230-1100 nm using a quartz absorbance microcuvette (Starna Cells, Inc.) with 1 cm path length. We chose this range in order to observe the absorbance of protein in our sample (around 275 nm) and the NIR absorbance of ICG (between 600-1000 nm).

Fluorescence spectra of NETs were obtained using a HORIBA Jobin Yvon Fluorolog-3 spectrofluorimeter in the range of 670-900 nm using a quartz fluorescence microcuvette (Starna Cells, Inc.) with 1 cm path length. Fluorescence

emission was induced in response to 650 nm excitation from a 450 W xenon arc lamp. We define the relative fluorescence intensity $\zeta(\lambda)$ as:

$$\zeta(\lambda) = \frac{F(\lambda)}{1 - 10^{-A(650)}}$$

where $F(\lambda)$ is the wavelength-dependent fluorescence intensity, and $A(650)$ is the absorbance at 650 nm excitation wavelength. All absorbance and fluorescence datasets were processed in Microsoft Excel. The relative fluorescence (Figure 3) was plotted and smoothed using 30 passes of the binomial smoothing algorithm in Igor Pro. The relative fluorescence intensity was then integrated and plotted in Figure 4 to report a measure of total NIR light emitted due to ICG fluorescence.

RESULTS AND DISCUSSION

The monomeric absorption peak of ICG (785 nm) does not change throughout the range of concentrations that was used to fabricate the NETs (Figure 2). The constant value of the protein absorbance at 275 nm suggests that the number of EGs being loaded in each sample was nearly the same.

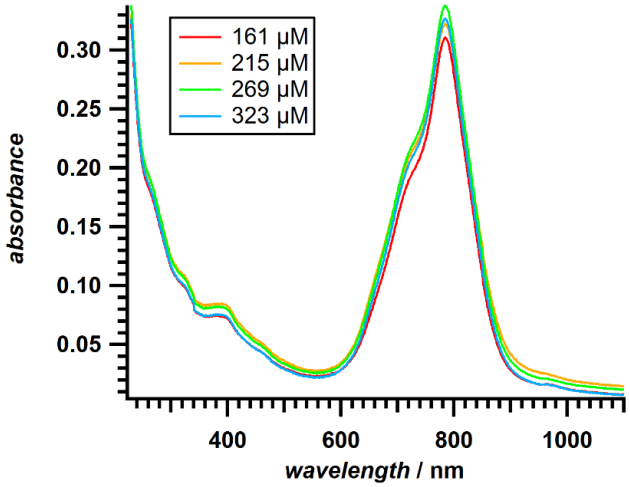

Figure 2: Absorbance spectra of NETs loaded with various concentrations of ICG (161-323 µM). There is a monomeric absorbance peak at 785 nm and a dimeric absorbance shoulder near 700 nm.

The relative fluorescence spectra show peaks at 700 nm (corresponding to the aggregated form of ICG) and 790 nm (corresponding to the monomeric form of ICG) (Figure 3). All spectra shown in Figures 2 and 3 are averages of three unique samples created using the same concentration of ICG.

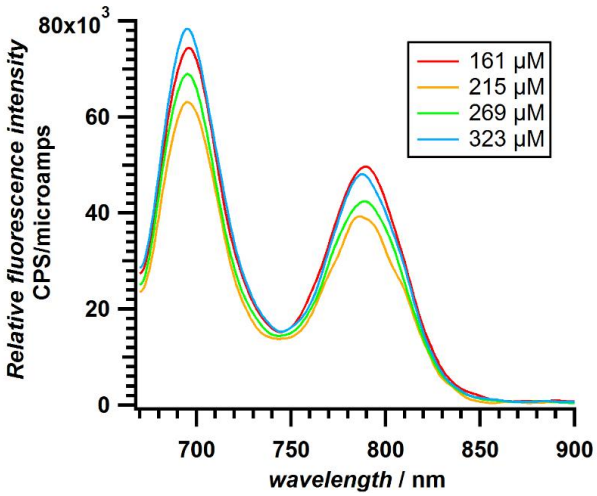

Figure 3: Fluorescence spectra of NETs fabricated using various concentrations2 of ICG (161-323 µM). Excitation wavelength was 650 nm. There is a peak at 700 nm corresponding to the emission of aggregated ICG. A second, smaller peak at 785 nm corresponds to the emission of monomeric ICG. Datasets were smoothed using 30 passes of a binomial smoothing algorithm in Igor Pro.

Fluorescence spectra shown in Figure 3 were integrated to yield the brightness of each sample of NETs (Figure 4). Three NET samples were fabricated at each concentration (consisting of 161, 215, 269, and 323 µM). We did not find any statistically significant difference among the integrated emission values for NETs fabricated using ICG concentrations in the range of 161-323 µM.

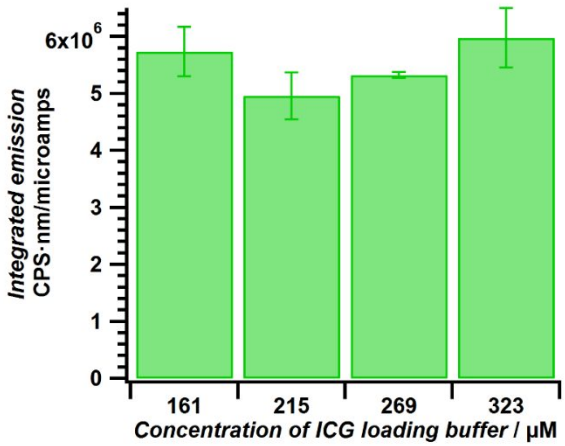

Figure 4: Integrated fluorescence emission of NETs fabricated using various concentrations of ICG (161-323 µM). Error bars are reported as +/- one standard deviation (n=3).

NETs fabricated using a range of ICG concentrations between 161 – 323 µM show similar absorption and fluorescence characteristics. These results suggest that there may be a limit to the amount of ICG that can be loaded into the NETs fabricated according to the protocol described in this paper. In our future studies, we will investigate the effect of using lower ICG concentrations.

ACKNOWLEDGEMENTS

This work was supported in part by grants from the National Science Foundation (CBET – 1403191), the American Society for Laser Medicine and Surgery, the University of California Cancer Research Coordinating Committee (5-441894-34912) and the Office of Research and Economic Development at UC Riverside.

REFERENCES

[1] Pansare, V. J., Hejazi, S., Faenza, W. J., and Prud'homme, R. K., "Review of Long-Wavelength Optical and NIR Imaging Materials: Contrast Agents, Fluorophores, and Multifunctional Nano Carriers," Chem. Mater. 24(5), 812-827 (2012).

[2] Fox, I. J., and Wood, E. H., "Applications of Dilution Curves Recorded from the Right Side of the Heart or Venous Circulation with the Aid of a New Indicator Dye," Proc. Staff M. Mayo Clin. 32(19), 541-550 (1957).

[3] Miller, E., Gleason, W. L., and Mcintosh, H. D., "Comparison of Cardiac Output Determination by Direct Fick Method and Dye-Dilution Method Using Indocyanine Green Dye and a Cuvette Densitometer," J. Lab. Clin. Med. 59(2), 345-350 (1962).

[4] Caesar, J., Sherlock, S., Shaldon, S., Chiandussi, L., and Guevara, L., "Use of Indocyanine Green in Measurement of Hepatic Blood Flow and as a Test of Hepatic Function," Clin. Sci. 21(1), 43-57 (1961).

[5] Oriock, D. A., Slakter, J. S., Ciaardella, A. P., Yannuzzi, L. A., Spaide, R. F., and Guyer, D. A., "Liver function and ophthalmic indocyanine green angiography," Invest. Ophthal. Vis. Sci. 40(4), S130-S130 (1999).

[6] Daly, R., and Potts, G., "Demonstration of Ophthalmic Artery and Choroid Plexus of Eye by Carotid Angiography," Neurology 13(2), 120-122 (1963).

[7] Schurr, P. H., "Angiography of the Normal Ophthalmic Artery and Choroidal Plexus of the Eye," Brit. J. Ophthal. 35(8), 473-478 (1951).

[8] Patel, J., Marks, K., Roberts, I., Azzopardi, D., and Edwards, A. D., "Measurement of cerebral blood flow in newborn infants using near infrared spectroscopy with indocyanine green," Pediatr. Res. 43(1), 34-39 (1998).

[9] Guo, W. B., Zhang, L., Ji, J., Gao, W., Liu, J. T., and Tong, M., "Breast cancer sentinel lymph node mapping using near-infrared guided indocyanine green in comparison with blue dye," Tumor Biol. 35(4), 3073-3078 (2014).

[10] Rossi, E., Hanna, R., and Boggess, J., "Sentinel lymph node mapping for cervical cancer using Indocyanine green and the da Vinci Si fluorescence imaging," Gynecol. Oncol. 125, S11-S11 (2012).

[11] Nakamura, Y., Fujisawa, Y., Nakamura, Y., Maruyama, H., Furuta, J., Kawachi, Y., and Otsuka, F., "Improvement of the sentinel lymph node detection rate of cervical sentinel lymph node biopsy using real-time fluorescence navigation with indocyanine green in head and neck skin cancer," J. Dermatol. 40(6), 453-457 (2013).

[12] Inoue, S., Shiina, H., Hiraoka, T., Wake, K., Sumura, M., Honda, S., Urakami, S., and Igawa, M., "A novel concept of sentinel lymph node in clinically localized prostate cancer by fluorescence navigation after intraoperative indocyanine green injection into prostate," J. Urology 179(4), 48-49 (2008).

[13] Polom, K., Murawa, D., Rho, Y. S., Spychala, A., and Murawa, P., "Skin melanoma sentinel lymph node biopsy using real-time fluorescence navigation with indocyanine green and indocyanine green with human serum albumin," Brit. J. Dermatol. 166(3), 682-683 (2012).

[14] Tanaka, R., Nakashima, K., and Fujimoto, W., "Sentinel lymph node detection in skin cancer using fluorescence navigation with indocyanine green," J. Dermatol. 36(8), 468-470 (2009).

[15] Arevalo, J., Mendoza, A. J., and Fernandez, C. F., "Photodynamic therapy with indocyanine green (i-PDT) combined with intravitreal triamcinolone acetonide for choroidal neovascularization," Invest. Ophthal. Vis. Sci. 44, U129-U129 (2003).

[16] Messmann, H., Baumler, W., Debl, K., Abels, C., Szeimies, R. M., Scholmerich, J., and Holstege, A., "Indocyanine green a new photosensitizer for PDT in human colon carcinoma cells? Intracellular uptake and phototoxic effects in vitro.," Gastroenterology 112(4), A614-A614 (1997).

[17] Bahmani, B., Bacon, D., and Anvari, B., "Erythrocyte-derived photo-theranostic agents: hybrid nano-vesicles containing indocyanine green for near infrared imaging and therapeutic applications," Sci. Rep. 3, 2180 (2013).

[18] Bahmani, B., Lytle, C. Y., Walker, A. M., Gupta, S., Vullev, V. I., and Anvari, B., "Effects of nanoencapsulation and PEGylation on biodistribution of indocyanine green in healthy mice: quantitative fluorescence imaging and analysis of organs," Int. J. Nanomed. 8, 1609-1620 (2013).

[19] Jung, B. S., Rao, A. L. N., and Anvari, B., "Optical Nano-Constructs Composed of Genome-Depleted Brome Mosaic Virus Doped with a Near Infrared Chromophore for Potential Biomedical Applications," ACS Nano 5(2), 1243-1252 (2011).

[20] Flower, R., Peiretti, E., Magnani, M., Rossi, L., Serafini, S., Gryczynski, Z., and Gryczynski, I., "Observation of Erythrocyte Dynamics in the Retinal Capillaries and Choriocapillaris Using ICG-Loaded Erythrocyte Ghost Cells," Invest. Ophthal. Vis. Sci. 49(12), 5510-5516 (2008).